Experimental Studies on Non-thermal Irreversible Electroporation in Tissue

Boris Rubinsky

Department of Mechanical Engineering, University of California, Berkeley, CA 94720 USA
and
Center for Bioengineering in the Service of Humanity and Society, School of Computer Science and Engineering, Hebrew University of Jerusalem, Givat Ram Campus, Jerusalem, Israel
Corresponding author E-mail: rubinsky@me.berkeley.edu, rubinsky@cs.huji.ac.il

Introduction

In the past, irreversible electroporation of tissue was studied for two applications: a) in the food industry for food processing and b) as a means to determine the upper limit of electrical parameters for reversible electroporation of tissue. Non-thermal irreversible electroporation (NTIRE) is a new modality for tissue ablation that applies the irreversible electroporation pulses in such a way as to avoid thermal damage to tissue components while irreversible affecting the cells. This particular aspect of irreversible electroporation was not studied before. This chapter reviews experimental studies on non-thermal irreversible electroporation in tissue done by our group. The studies will be discussed in the chronological order in which they were done. In all the studies discussed in this chapter, treatment planning was done prior to performing the experiments. Treatment planning is done to identify the appropriate sequence of electrical pulses, which produce the desired cell ablation without causing damage to the remaining tissue structure, [1]. It is not trivial as the range of parameters used can vary from tissue type to tissue type and from circumstance to circumstance. In the absence of other information, in these earlier studies modeling the electrical field and the temperature distribution caused by Joule heating during the application of the electrical pulses identified the treatment planning. It is possible that in the future it will be also valuable to model that change in pH in the tissue, as they could also affect the tissue components, e.g. [2]. It should be emphasized that when thermal or chemical damage do occur during irreversible electroporation, the outcome of the procedure will most likely be different from those described in this chapter.

NTIRE of the Liver

The first two papers in this area have studied NTIRE in the liver, [3], [4]. The liver is a highly vascular organ and has served often as the preferred organ for studying methods for minimally invasive surgery, e.g. [5], [6]. Main reasons for studying minimally invasive ablation techniques in the liver, in addition to its relative homogeneity, are the value of minimally invasive tissue ablation in treatment of liver cancer and the difficulties in performing conventional resection surgery in this organ.

B. Rubinsky (Ed.): Irreversible Electroporation, BIOMED, pp. 155–181.
springerlink.com © Springer-Verlag Berlin Heidelberg 2010

The experiments reported in [3], were performed on the liver of Spraque Dawley rats. The 10 mm diameter and one mm thick electroporation electrodes were made of sintered Ag/AgCl (E255, *In Vivo Metric*, Healdsburg, CA). While in conventional electroporation it is more common to use stainless steel electrodes, in this study Ag/AgCl was used because one aspect of our research is to evaluate the changes in electrical properties of tissue during and after electroporation for use in monitoring and controlling electroporation [6], [7]. The lobe of the liver was clamped between the two electrodes placed in contact with the liver in such a way that the liver was sandwiched between the two parallel cylindrical surfaces of the electrodes. The NTIRE protocol was developed through treatment planning and consists of one 20 ms pulse of 400 V delivered across 4 mm of liver. Roughly this corresponds to 1000 V/cm. However, it should be emphasized that in the complex geometry of real tissue the geometry and configuration of the tissue and of the electrodes should be carefully considered and analyzed. Evaluating the electrical fields only from the voltage difference between the electroporation electrodes is only roughly indicative of the actual electrical fields, the temperature and the thermal damage which occurs during the electroporation [1], [9], [10].

The pulse was delivered with a commercial pulse generator (ECM 830, *Harvard Apparatus*; Holliston, MA). The animal was observed continuously while in thermal incubation until three hours after pulsing. At this point, the animal was euthanized. To fix the liver at its current state for microscopic viewing, we flushed the vasculature with physiological saline for ten minutes at a hydrostatic pressure of 80 mmHg from an elevated IV drip. Injecting the fluid into the left ventricle and letting it exit from a cut made in the right atrium accomplished this. Dr. Narayan Raju designed this tissue fixation type procedure. We have found that flushing the tissue prior to fixation can produce valuable insight into the mechanisms of action of NTIRE in relation to its effect on the blood vessels. Immediately following saline perfusion, a formaldehyde fixative was perfused in the same way for ten minutes. The treated liver lobe was then removed and stored in the same formaldehyde. Hematoxylin-eosin staining was then performed on cross-sections through the center of the treated region to elucidate the microscopic morphology.

Figure 1 presents the highlights of our findings. Figure 1a, shows a macroscopic view of the treated liver (one half plane). The dark circular region is the area affected by NTIRE. It corresponds to the dimension of the electroporation electrodes. A rim of thermal damage was observed on the surface of the liver. It corresponds to the edges of the electrodes and it is due to the high local fields. It could be avoided by using rounded edge electrodes. Figures 1b and 1 c show the mathematical calculations of the electrical field and the temperature distribution superimposed on a macroscopic tissue cross section made through the central plane of the lesion and demonstrates that the lesion is non-thermal irreversible electroporation. The figure shows that the ensuing electric field from the pulse is fairly uniform in the area directly between the electrodes at about 1kV/cm. The electric field drops precipitously as the distance from the electrode axis exceeds the electrode radius and approaches zero near the outer edges of the liver. When analyzing the electric field contours it is important to notice the 600 V/cm to 700 V/cm contours. This has been also determined in previous studies with the rabbit liver as the parameters of demarcation between reversible and irreversible

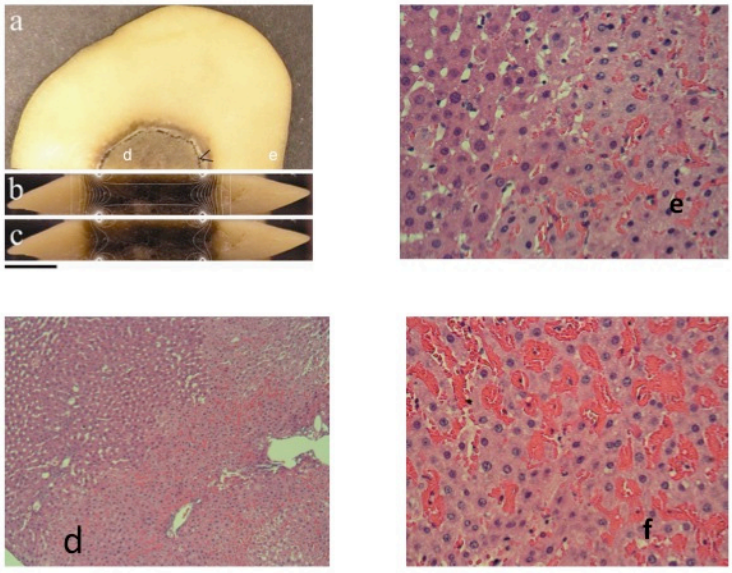

Fig. 1. NTIRE treated liver. (1a) Top view of the treated liver. Thin semicircle of thermally ablated tissue is visible near the extents of the tissue ablated by irreversible electroporation (dark area). (1b) Electric field strength resulting from the 400 V pulse. Lines of constant electric field strength are superimposed upon the side view of this liver. The lines represent 100 V/cm increments from 100 V/cm to 2000 V/cm, where the lowest values are at the far left and right edges and the highest occur within an annular region corresponding to the semicircle referred to in the top view. Two lines that cross the central region are 1000 V/cm contours. (c) Temperature rise due to Joule heating at the end of the 20 ms pulse. Lines of constant temperature are superimposed upon the same side view. The contours represent 1 °C increments from 38 °C to 50 °C where the lowest values are at the far left and right edges (ΔT is proportional to the square of the local electric field strength). The annular region where temperatures exceed 50 °C corresponds to the area that experienced thermal ablation (arrow), while the remaining effects were non-thermal in nature. Bar indicates 5 mm in all photos. Figures 1d,1e,1f: Histological effects of the irreversible electroporation pulse. (1d) and (1f) show the margin of ablation in 10x and 40x resolutions respectively. (1f) shows the core of the ablated region.

electroporation [11]. This indicates that irreversible electroporation was likely to have occurred in the region directly between the electrodes. Figs 1d and 1e, show the margin of the treated region (upper left hand corner is the untreated region). The figures show that the pale regions in Figs 1a, 1b and 1c correspond to a lack of red blood cells caused by the fixation procedure which flushed the vasculature with saline and then formaldehyde. Indeed, histology shows no damage to the hepatocytes or endothelial cells in this region. The cytosol is normal, the plasma membranes are distinct and the nuclei are healthy. In addition, the endothelial cells appear to have maintained their structural integrity since there were no leaks of red blood cells into the surrounding sinusoids. Moreover, this area resembles closely the control samples of liver in every way. Histological analysis revealed

acute damage to the tissue in treated regions. In central treated areas, Fig 1f, widespread pale eosinophilia and congestion in the sinusoids was evident. In some areas this congestion was so dense as to suggest the intercellular adhesion between adjacent hepatocytes had been impaired. Massive diapedeses and early fibrin deposition also occured within the sinusoids. These conditions would likely have caused coagulative necrosis of the hepatocytes. Additionally, vacuolar degeneration of hepatocytes was present throughout the central treated region, but occurred most significantly in centrilobular areas, further suggesting an interruption of blood flow and oxygen supply which resulted in ischemic damage.

At the margins of treated areas various stages of cellular degeneration were present. In all cases, the treated side exhibited pale eosinophilic cytoplasm when compared with the untreated side. In some areas, moderate pyknosis of the nuclei and sinusoidal congestion were present in the treated side and conspicuously absent in the other side. Cell borders were also clearly visible on the non-treated side and nearly indistinguishable in the treated side. This suggests that the primary expected consequence of the procedure had occurred: cell membrane disruption. In other areas, obvious vacuolar degeneration marked the boundary between healthy and pathological parenchyma. The line of demarcation was often surprisingly narrow (between adjacent hepatocytes), but did not correspond to lobular boundaries. Throughout the treated area, insult to endothelial cells was evident. In nearly all cases, endothelial necrosis was present and large numbers of neutrophils were marginated along and had infiltrated within the vessel walls, indicating acute vascular inflammation. Erythrocytes were also seen pooling immediately beneath the endothelium. Notably, at three hours after treatment, this vascular necrosis had not destroyed large blood vessel architecture as indicated by the successful flushing of blood from these vessels (clear lumen), Fig 1d.

The goal of this first NTIRE study was to determine through in-vivo experiments in rat liver if sufficiently strong electric pulses cause non-thermal and controllable ablation as a consequence of irreversible electroporation alone. The results suggest that irreversible electroporation can be used to ablate large volumes of tissue in a controlled manner and with a sharp boundary between necrotic and unaffected tissue. In addition, the tissue fixation procedure we have employed showed that irreversible ablation can cause occlusion of small blood vessels (sinusoids) and their congestion with crenated red blood cells. Related effects of reversible electroporation on blood flow were found previously, though if reversible electroporation has occurred in those cases they differ with what we have found [12,13,14,15]. This finding has important applications. It suggests that in the irreversible electroporated region any cell that may survive electroporation would experience ischemia and death through oxygen depravation. An intriguing use of the congestion of red blood cells could be in the entrapment of any type of drug inside the irreversible electroporated tissue. Injection of any drug or medical imaging contrast agent in the vasculature or in the interstitial space prior or during irreversible electroporation will cause the entrapment of the drug in that area. This way a bolus of high concentration drugs could continuously diffuse from the tissue in which it is entrapped and act focally in the irreversible electroporated area and around it or a concentrated area of imaging contrast agents could identify the treated region.

Perhaps the most important finding of this study is that the large blood vessels architecture is intact after non-thermal irreversible electroporation, while the cells around it are ablated. This is the unique consequence of non-thermal ablation and is perhaps the most important attribute of NTIRE, which distinguishes it from other ablation techniques. Other tissue ablation techniques non-discriminately affect all the organic molecules in the treated volume. As a consequence the blood vessel architecture is also damaged. Because NTIRE affects only the cell membrane the extracellular architecture remains intact and the scaffold of the blood vessels, ducts and any other structures that are not cells remains intact. The mechanical integrity of the tissue is retained. This has major significance in treatment of cancer. One of the major difficulties in ablating cancer abutting large blood vessels or important duct structures is the fact that thermal treatment cannot be used to affect cells near blood vessels because of the thermal effect of the vessels on one hand and because the thermal ablation impairs the larger blood vessels on the other. The ability of irreversible ablation to cause cell necrosis near the vessels while preserving the large vessel architecture could be used to treat tumors near the larger blood vessels and complex structures of the tissue. This result also suggested to us the use of NTIRE in treatment of restenosis, a study that we will discuss later.

The first long term, large animal study of NTIRE was reported in [4]. The goal of that study was to test the NTIRE tissue ablation treatment planning based methodology in the pig liver and to provide results on long term histopathology of NTIRE ablated tissue. Prior to experiments, treatment planning was done through a mathematical analysis of the electrical field in the treated area as well as the temperature distribution, which is produced by Joule heating during treatment (Figs 2a,2b). This study was conducted in accordance with Good Laboratory Practice regulations as set forth by the 21 Code of Federal Regulations (CFR) Part 58. Each procedure started with anesthetization of the animal under general anesthesia per SOP #33156. It is very important to notice that upon application of the NTIRE pulse a variable degree of generalized muscle contraction occurred in each animal, from no contraction to mild to moderate contraction. The degree of contraction appeared to be related to the level of anesthesia of the animal the degree of muscle blocking agents given, if any, and the voltage of the pulse used. In general we found that when Pancuronium was administered to the pig the contractions were manageable even when fields of 3kV were applied to the electrodes. It appears that voltages lower than 1.5 kV produced little to no contraction in anesthetized animals. Therefore, pancuronium (0.1 mg/kg, at a dose of 1 mg/ml) was administered through an IV prior to the procedure, to reduce muscle contractions during the application of the electrical pulses. Pancuronium (0.05 mg/ml at 1 mg/ml) was administered throughout the procedure as needed. The liver was exposed via a midline incision (see Fig. 1C). IRE was performed using 18 gauge stainless steel electrodes (Oncobionic Inc., USA) with a sliding insulating sheath exposing 1 cm of electrode. The electrodes were inserted in the liver under ultrasound monitoring in configurations of either two or four electrodes in a roughly axial parallel configuration. Figure 1D illustrates the insertion of the four needle electrodes using an insertion template. Square DC pulses were applied to the liver through the electrodes using a DC pulse generator (IGEA Co., Italy). The pulse was delivered in a bipolar manner between two electrodes. Lesions made using the four electrode configurations had overlapping lesions created by activating the electrodes in different bipolar configurations

between the four electrodes. The parameters that were varied in this study were the voltage, the distance between the electrodes, and the number of pulses. The number of pulses varied between two and eight, 100 microsecond pulses. Between four and twelve lesions were produced in the liver of each animal. The treatment planning and the introduction of the electrodes in this study are shown in Fig 2. An explanation of the results is given in the figure legend.

An interesting finding with significance to NTIRE is shown in Fig 3. The insertion of the needles was done under ultrasound monitoring and the procedure was subsequently followed by ultrasound. Since NTIRE is a minimally invasive procedure the use of medical imaging for treatment of tissues inside the body is highly recommended. In Figure 3A axial ultrasound shows four bright

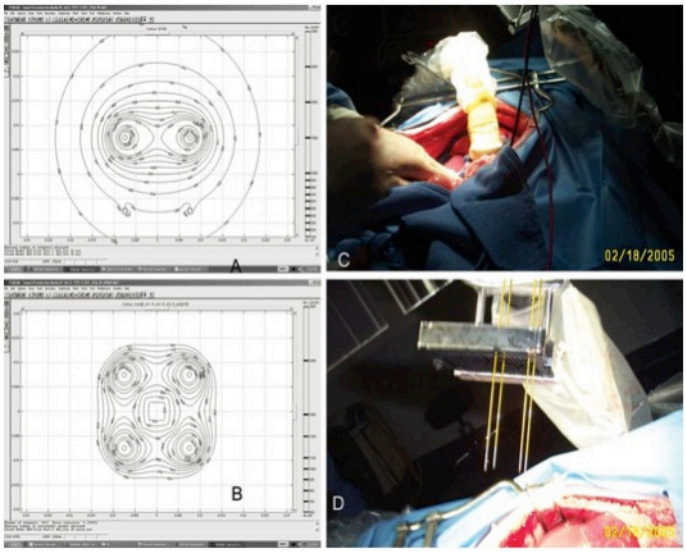

Fig. 2. Treatment planning and surgical protocol for irreversible electroporation ablation in the pig liver. IRE pulse parameters are bipolar electroporation, 2.5 kV pulses applied in a train of eight 100 microsecond pulses separated by 100 milliseconds. Four electrodes 18 gage stainless steel electrodes, 1.5 cm distance between probes. (A) Results of mathematical analysis showing constant electrical field magnitude isolines during the application on an electroporation pulse between two electrodes. The numbers on the figures indicate the magnitude of the electrical field in increments of 100 V/cm starting from 100 V/cm (outer isoline). The power delivered during each pulse is 1.2 J per cm depth of electrode. (B) Results of mathematical analysis show constant electrical field magnitude isolines due to the superposition of the application of the IRE pulses between the four pairs of IRE electrodes. The numbers on the figures indicate the magnitude of the electrical field in increments of 100 V/cm starting from 600 V/cm (outer isoline). Experiments have shown that 600 V/cm induces irreversible electroporation in liver. (C) Photograph of application of electroporation probes with ultrasound, (D) insertion of a set of four electrodes. [4]

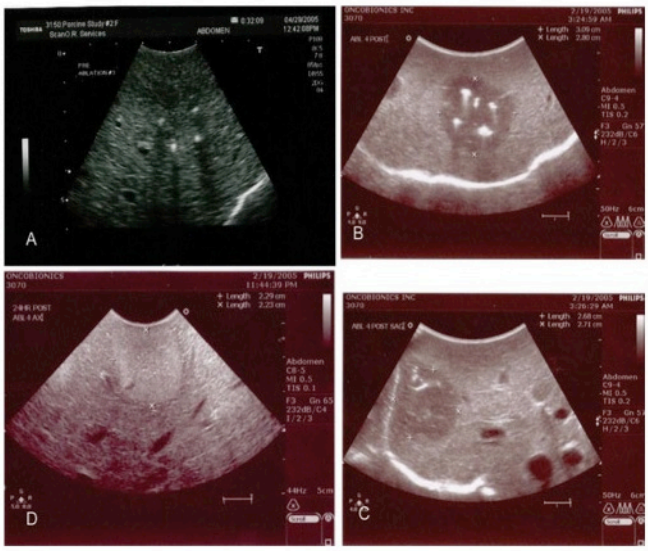

Fig. 3. Ultrasound images of an IRE process: a) during the insertion of the needles (bright spots), b) and c) Immediately after the delivery of the electroporation pulses d) 24 hours later. [4]

hyperechoic dots representing the four needle tracks. Most interesting was the finding that immediately following pulse application ultrasound showed a markedly hypoechoic lesion in the expected location of the IRE lesion [Figs. 3B (axial) and 3C (sagital)]. Subsequent studies show that this effect is more pronounced in vascular tissues and can be seen on any imaging technology, such as CT, ultrasound and MRI. At 24 hours the ultrasound image showed the hyperechoic lesion had changed character and was now uniformly hyperechoic. Figure 3D is the sagital view after 24 hours that corresponds to Figure 3C.

To fix the liver in its current state for microscopic viewing, a Foley catheter was placed into each branch of the portal vein and hepatic veins and the liver was flushed the with physiological saline for ten minutes at a hydrostatic pressure of 80 mmHg from a pressurized IV drip. Immediately following saline perfusion, a 5 % formaldehyde fixative was perfused in the same way for ten minutes. The liver lobe in which the IRE lesion was made, was then removed and stored in the same formaldehyde solution. For macroscopic analysis the tissue was bread loafed perpendicular to capsule surface and parallel to the needle tracts. All cassettes were processed routinely from 10% Phosphate Buffered Formalin to wax blocks. Five micrometer sections were made from each block and stained with Hematoxylin and Eosin for histologic examination. Some cassettes were also stained with Von Kossa stain for calcium detection. The goal of the histopathology was to verify the extent and the nature of tissue ablation with IRE; in particular, in relation to the margins of the treated zone, blood vessels and other vascular structures, and the long-term resolution of the lesions.

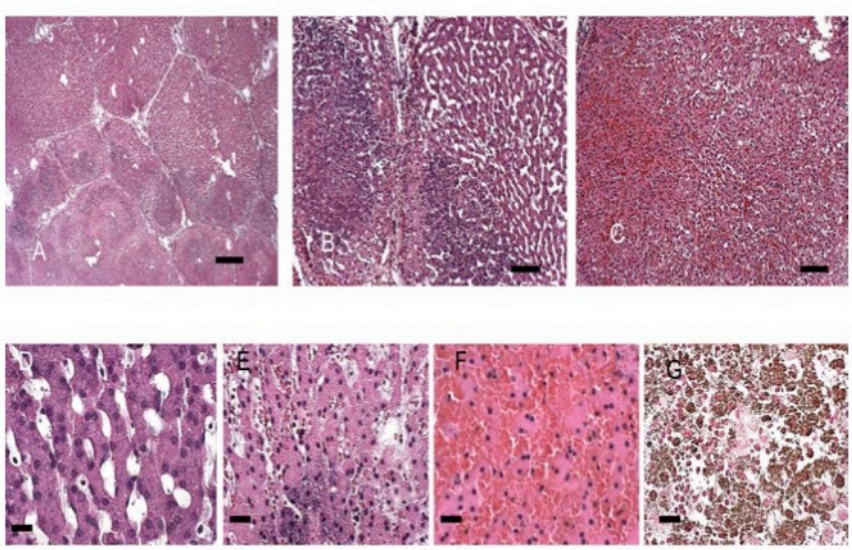

Fig. 4. Microscopic histology of IRE ablation in the pig liver, 24 hours post IRE. (A) H&E stained section. Margin of ablated area (bottom half) and unaffected area (top half). Focal dark areas are necrotic hepatocytes with calcification. Scale bar 500 micron. (B) H&E stained section. Margin of ablated area (left) and unaffected area (right). Focal dark areas are necrotic hepatocytes with calcification. Scale bar 100micron. (C) H&E stained section. Central area of ablation. Hepatocytes have hypereosinophilic cytoplams and pyknotic nuclei. Sinusoids are congested. Scale bar 100 micron. (D) H&E stained section. Normal area of hepatic parenchyma for comparison to ablated region. Scale bar 25 micron. (E) H&E stained section. Area of hepatic necrosis with hypereosinophilic cytoplasm and pyknotic nuclei. Aggregate of hepatocytes at bottom also contain calcium. Scale bar 25 micron. (F) H&E stained section. Area of hepatic necrosis with hypereosinophilic cytoplasm and pyknotic nuclei. Hepatocytes are separated by hemorrhage. Scale bar 25 micron. (G) Von Kossa stained section. Brown granular pigment is calcium in areas of hepatic necrosis of ablated region. Scale bar 25 micron. [4]

Figure 4 shows the microscopic appearance of the ablated tissue at different locations and magnifications at day one after the procedure. The gross lesion appears hemorrhagic. Histology shows the ablated area with diffuse necrotic hepatic parenchyma and no obvious viable tissue within the ablated zone. Needle tracts form 1-2 mm holes filled with blood and fibrin. The ablated zone is well demarcated and non-encapsulated from the immediately adjacent unaffected hepatic parenchyma with an abrupt transition between necrotic hepatic parenchyma in the ablation area and adjacent normal hepatic parenchyma. The central region of the treated area has coagulation necrosis of hepatocytes. The hepatocytes have hypereosinophilic cytoplasm and pyknotic to karyolitic nuclei and in some areas contain basophilic granular intracytoplasmic material (calcification) and loss of cellular detail. Sinusoids in this area had congestion admixed with fibrin and small to moderate numbers of inflammatory cells (neutrophils and eosinophils). Within

the lesion, portal vessels and bile ducts had variable signs of wall necrosis but appeared structurally intact. Many larger bile ducts were intact. Necrotic vessels in the ablated area had variable loss of endothelium and are surrounded by scattered red blood cells (hemorrhage), neurophils, and eosinophils and edematous stroma. In some areas the vessel walls are hypereosinophilic and homogenous consistent with fibrinoid necrosis. Occasional affected vessels have organized intraluminal fibrin thrombi. Moderate mixed inflammatory cells and edema are present in portal stroma and adjacent to affected portal vessels with extension into perilobular stromal connective tissue. The peripheral region of the ablated zone has similar necrotic lobules as described more centrally. In some areas, necrotic hepatocytes had intracytoplasmic basophilic granular material consistent with dystrophic calcification. This is most prominent at the margin of the ablated area with some cells completely replaced by calcification. The region outside the ablated zone is unremarkable except for occasional portal zones showing occasional lymphocytic infiltrates. The margin of the ablated area has increased inflammatory cells characterized predominantly by moderate to large numbers of neutrophils and lesser numbers of eosinophils, lymphocytes and macrophages.

Figure 5 illustrates the long-term effects of NTIRE on the liver. Day 1, post IRE ablation results are consistent with those above. Particular here is a large vein at the deep margin of the ablated area. Ablation extends up to this vein. The vessel is unremarkable. The regional lymph node has mild cortical reactivity and expansion of medullary sinuses consistent with a drainage reaction. Medullary sinuses are expanded by red blood cells, eosinophils, neutrophils, and macrophages. Paracortical regions are expanded by increased lymphocytes. Occasional lymphoid follicles have reactive germinal centers. This is surrounded by fibrosis admixed

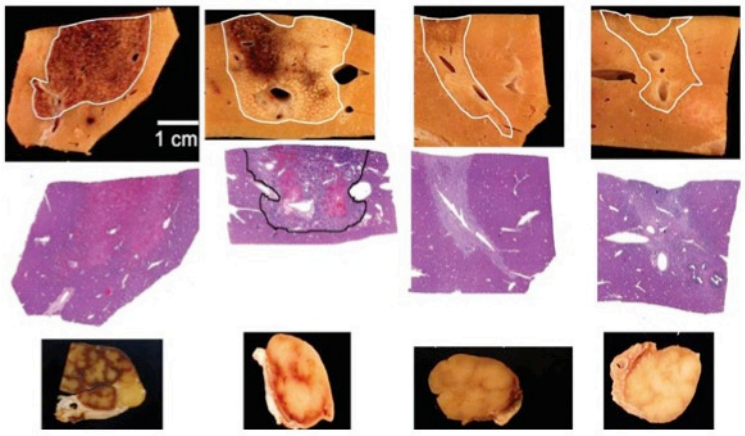

Fig. 5. Each column of figures shows: top macroscopic gross histology, middle macroscopic H&E histology, and bottom lymph node. The first columns from right is for 1 day post IRE ablation pulse, the second three days, the third seven days, and the fourth fourteen days. (The outline of the affected area is marked) [4]

with macro-phages and lymphocytes. Within this particular lymph node, there is a well demarcated chronic, eosinophilic granuloma measuring approximately 0.5mm in diameter surrounding a mineralized core. The origin of the mineralization is unknown, but is compatible with a necrotic parasite reaction. In this liver sample, eosinophils were also part of the inflammation. These are usually associated with parasitic infections and dermatologic disorders and the mineralization may explain the eosinophils in this animal series. We observed substantially enlarged lymph nodes in all our animal experiments. Therefore, it is possible that the eosinophils are mediated by unknown immunogenic factors related to the IRE treatment. Nevertheless, because of the results in this animal we cannot determine the cause with certainty.

Day 3, post treatment affected area is continuous with a central hemorrhagic, necrotic zone and variable loss of hepatic architecture. The continuous area is irregularly demarcated and non-encapsulated from adjacent unaffected hepatic parenchyma. Within the deep part of the ablated area and at one lateral margin there are two large veins. The ablation changes extend up to the vessels. Vessels are patent, surrounded by stromal edema and have variable necrosis of endothelial cells lining the intima. The integrity of the larger blood vessels is typical to NTIRE and it is an important attribute of this technique. The central hemorrhagic regions has diffusely necrotic lobules with marked congestion (hemorrhage), fibrin, and variable loss of hepatocyte cellular architecture. There are also multifocal chords of necrotic hepatocytes with diffuse replacement by basophilic material (calcium). The more peripheral affected regions consist of lobules with increased cellularity and loss of sinusoidal architecture (regenerative nodules). The regenerative nodules replace lobules that were overall necrotic at day 1, post treatment. Cells within these lobules are pleomorphic (spindle to oval to polygonal) and are consistent with regenerative hepatocytes that are extending from the lobule/stroma margin admixed with mixed inflammatory cells. The interlobular stroma has marked increase in fibrosis with marked bile duct proliferation throughout. Bile ducts are irregular and occasional mitotic figures are present. Most ducts contain intraluminal neutrophils, eosinophils, and necrotic cellular debris. The stroma contains proliferative fibroblasts, increased small veins and capillaries, and mixed inflammation consisting of macrophages, lymphocytes, eosinophils, and neutrophils. The regions outside the ablated area have multifocal portal areas with small numbers of lymphocytic infiltrates but are otherwise unremarkable. Eosinophils are part of the overall inflammation. These are usually associated with parasitic infections and dermatologic disorders. It is also possible that they may be mediated by unknown factors related to IRE ablation. The lymph node shows medullary sinuses expanded by eosinophils, neutrophils, lymphocytes, macrophages, and lesser numbers of scattered red blood cells. Paracortical regions are expanded by increased lymphocytes. Occasional lymphoid follicles have reactive germinal centers.

At seven days post treatment, the affected area is continuous with similar changes throughout. The ablated area is irregularly demarcated and non-encapsulated from the immediately adjacent unaffected hepatic parenchyma. The lateral margins of the affected area taper inward (affected area is contracted) as

expected with increased fibrosis (scarring). Hepatic lobules have been replaced by regenerative hepatic nodules that are undergoing hepatic vacuolar degeneration. Nodules are variable in size surrounded by dense fibrous stroma. Nodules consist of diffuse hepatocytes with no sinu-soidal architecture. Hepatocytes are swollen, have increased clear to granular cytoplasm and pyknotic nuclei (vacuolar degeneration). The stroma contains increased bile ducts that are overall intact and unremarkable (less proliferative than at three days post treatment). It also contains increased small to medium size veins and capillaries (compared to three days post treatment). The stroma shows proliferative fibroblasts and mixed inflammation consisting of macrophages, and lymphocytes. A large vein runs through much of the ablated area. This vein has variably necrotic endothelium with some sloughing of endothelial cells. The lumen is patent. Ablated area extended to vessel wall. The regions outside the ablated area have multifocal portal areas with small numbers of lymphocytic infiltrates but are other wise unremarkable. The lymph node shows medullary sinuses that are expanded by eosinophils, neutrophils, lymphocytes, macrophages, and lesser numbers of scattered red blood cells. Paracortical regions are expanded by increased lymphocytes. Multifocal lymphoid follicles have reactive germinal centers.

By 14 days the ablated lesions are difficult to identify. The affected area is almost completely replaced by fibrous scar tissue. Scattered throughout the fibrous stroma are many profiles of bile ducts as well as many variably sized vessels consisting predominently of veins and capillaries. The stroma in the affected area contains moderate aggregates and scattered inflammatory cells consisting of lymphocytes, plasma cells, and macrophages admixed in some areas with red blood cells. Rare individual and aggregates of viable hepatocytes are present within the fibrous stroma (in most areas close to the margin of viable hepatic lobules). The stroma also contains scattered individual and aggregates of swollen vacuolated cells with pyknotic nuclei (hydropic degeneration) consistent with hepatocytes seen in regenerative nodules at seven days post treatment. It was felt by our pathologist that this was part of the regenerative process, but the possibility that these were untreated viable heptocytes could not be ruled out. The adjacent viable hepatic lobules had peri-lobular fibrosis and mild to moderate chronic peri-portal inflammatory infiltrates. Focal areas of mineralization were identified throughout the scar and were consistent with dystrophic calcification or osseous metaplasia. The periportal lymph nodes were again enlarged with similar features to those at seven days; however, germinal centers contained greater numbers of macrophages consistent with a chronic lymphoid reactivity.

In summary, histology shows that the IRE ablated area is continuously necrotic, with an abrupt transition, several cell layers thick, between treated necrotic hepatic parenchyma and the adjacent untreated normal hepatic parenchyma. Larger vascular structures are mainly intact. A unique aspect of IRE is the mechanisms of cell ablation. In IRE when cells are exposed to a pulsed electrical field with the proper parameters, irreversible nano-scale defects are created in the cell membrane and the cell loses its} homeostatic mechanisms. However, IRE does not affect connective structures, or denatures molecules, and collagen. This selective targeting of the cell membrane by IRE has important clinical implications. Since IRE affects only cell

membranes injuries to tissue scaffold are eliminated. Our pathology demonstrated intact bile ducts within the lesions. If successfully translated into clinical practice this could have major implications by markedly decreasing the incidence of biliary complications associated with hepatic tumor ablations. Other organs could also benefit from this property of IRE. In the prostate this could translate into significantly less chance of urethral damage and in the kidney less chance for damage to the collecting system. IRE could also be promising for treatment of pancreatic cancer by producing no effects on the structures surrounding the pancreas. In the brain it could be used to treat tumors near large blood vessels.

Preservation of vasculature in an IRE lesion also has important clinical implications. Due to this intact vasculature lesions can heal throughout their volume simultaneously with amazing rapidity. Our experiments show almost complete lesion resolution in two weeks time. It would be expected that tumors with significant vascularity such as renal, breast, prostate, and hematomas might have very rapid resolution, while a vascular tumors such as colon metastases might resolve in longer periods of time. Rapid lesion resolution beyond making treatment efficacy easier to assess has significant clinical implications in situations where rapid decrease in the volume of the ablated zone is desirable such as the prostate, benign fibroadenomas of the breast, and myomas of the uterus. Rapid resolution of lesions without protein denaturation results in another unexpected pathologic finding related to an immunologic reaction in the lymph nodes draining the area of the ablation. All animals showed an obvious peripheral lymphadenpathy in the drainage area of the ablated tissue with microscopic evidence for associated inflammatory response. If an IRE treated tumor specific reaction in draining lymph nodes can be harnessed it could have implications for tumors that are known to spread via draining lymph nodes such as breast and prostate cancer. Such a reaction in lymph nodes draining an area of cancer could result in destruction of micrometastasis in the effected lymph nodes, which could significantly effect survival in melanomas, colon cancer metastatic to liver, breast cancer, and prostate cancer, to name a few.

The finding that IRE produces a lesion within liver with uniform necrosis throughout and to the very margins of the lesion and with a very narrow zone of transition from complete necrosis to normal liver is consistent with the selective mechanism of ablation of IRE and should provide accuracy in clinical tissue ablation. IRE lesions show complete destruction of tissue extending directly up to the vessel wall without sparing of tissue adjacent to the vessel. In addition, this was accomplished without vessel destruction or occlusion. This has major implications, in the liver, where local recurrences near vessels have been an ongoing clinical limitation of thermal ablation and to other tumor situations such as in centrally located kidney lesions where major vascular structures have also been problematic in producing a reliable ablation.

In addition to the histological findings the results of the long term study have confirmed that the extent of tissue damage by IRE is consistent with mathematical predictions and therefore, treatment planning is valuable for the design of IRE treatments. Additional findings are that there is value in increasing the number of

pulses to increase the size of the treated tissue, up to 100 pulses delivered in such a way as to not produce thermal effects were reported in that study.

NTIRE of the Prostate

A potentially important application of NTIRE is in the treatment of prostate cancer and benign prostate hypertrophy (BPH). An experimental study on the use of NTIRE in the prostate was reported in [16]. The study reported in [16] is limited in the number of animals tested and the parameters used and much more work remains to be done in developing optimal NTIRE parameters for the prostate.

Six male beagle dogs had their prostates treated using IRE. Each procedure started with anesthetization of the animal under general anesthesia per SOP #33156. In addition, as with all large animal experiments, pancuronium (0.1 mg/kg,) was administered through an IV prior to the procedure, to reduce muscle contractions during the application of the electrical pulses. Pancuronium (0.05 mg/ml at 1 mg/ml) was administered throughout the procedure as needed. Using trans-rectal ultrasound 18 gauge electrodes were placed transperennially into the prostate in 3 dogs. Two to 4 probes were placed into one lobe of the prostate in 5 dogs. In 2 dogs, 4 probes were placed in order to create a hemi-ablation of the prostate. The probes were used in pairs of two, and each pair applied 80 pulses of 1500, with a pulse length of 100 microseconds. In the sixth dog pairs of probes were placed to purposely create a lesion in certain sensitive structures such as the urethra, rectum and neurovascular bundles. Pulses applied in the safety study at each anatomical structure were 80 pulses of 2000 V with a pulse length of 100 microseconds. Pulses were applied using a DC generator (IGEA Inc.) that delivered pulses in the microsecond range of duration, with a variable pulse interval and voltage range. When IRE was delivered in a bipolar manner between two probes they were separated by between 1 and 1.5 cm. In three subjects a single probe with both electrodes incorporated into it and separated by 5mm was placed trans-rectally using ultrasound guidance. Treatment parameters of the single probe were 1 or 8 pulses of 1000 V with a pulse length of 100 microseconds. Pulses delivered per lesion varied in number. Three animals sacrificed at one day had 8 pulse delivered at 1 kV and two animals sacrificed at 2 weeks had 80 pulses delivered per pair of electrodes using 1.5 kV. The duration of the pulses was 100 microsecond with an interval between pulses of 100-200 milliseconds. Upon application of the IRE pulse a variable degree of generalized muscle contraction occurred in each animal, from no contraction to mild to moderate contraction. The degree of contraction appeared to be related to the level of anesthesia of the animal, the degree of muscle blocking agents given, if any, and the voltage of the pulse used, with the higher voltages causing greater contractions.

At day one the lesion made at 1 kV with 8 pulses appeared grossly to be hemorrhagic in the treated area (Figure 6A). Histology showed the ablated area to have diffuse necrotic glandular tissue with no obvious viable tissue within the ablated zone (Figure 6C). The ablated zone was well demarcated from the immediately adjacent unaffected prostate parenchyma with an abrupt transition between necrotic glandular tissue in the ablation area and adjacent normal glandular tissue

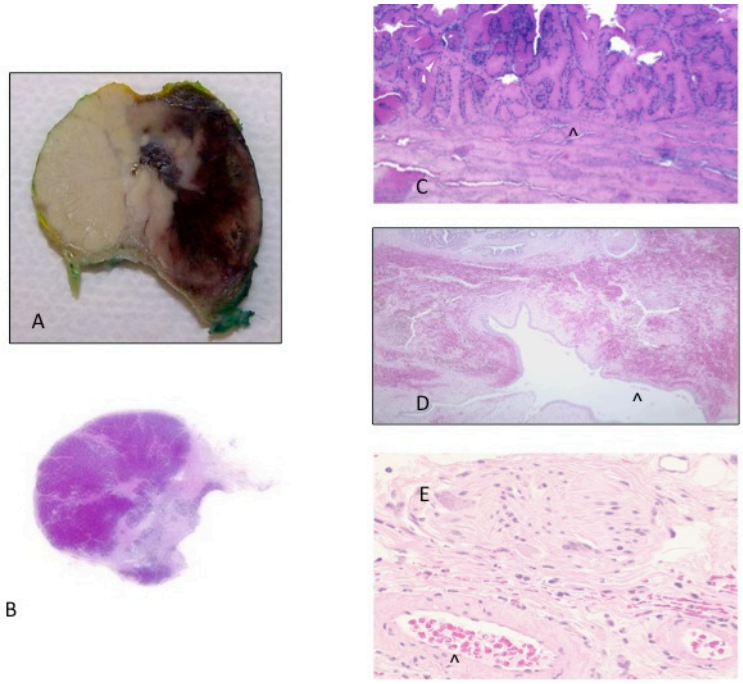

Fig. 6. 6A -Gross pathology of the IRE lesion at 24 hrs. The right side of the gland is hemorrhagic. (Pulses=8, 1.5 kV), 6B- Whole mount slide of a prostate where the right side of the gland was electroporated 2 weeks prior. There is marked shrinkage of the lobe with replacement by fibrous tissue (Pulses=80, 1.5 kV), 6C- Photomicrograph of prostate tissue that has been electroporated at 24 hrs. Photomicrograph at the margin of the IRE lesion. A very narrow zone of transition between normal and necrotic tissue is noted at the margin No glandular elements are visible (Pulses=8, 1.5 kV), 6D- The urethra is noted at the center of the micrograph as the open space at 24 hrs. Sub-mucosal hemorrhage is noted but the integrity of the urethra is still intact Pulses =8, 1.5 kV. 6E- Photomicrograph of the neurovascular bundle after electroporation at 2 weeks (Pulses=80, 1.5 kV). It can be seen that both the vessel and the nerve trunk show no evidence for necrosis. [16]

(Figure 6C). Necrotic glandular tissue was noted adjacent to the urethra however the urethral structural integrity remained intact without evidence for necrosis within the sub-mucosa (Figure 6D), even when the urethra was subjected to direct ablation during the safety portion of the study. In the neurovascular bundle areas, including the neurovascular bundle that was directly ablated during the safety portion of the study, vessels had variable loss of endothelium and were surrounded by scattered red blood cells (hemorrhage), neurophils, and edematous stroma. In some areas the vessel walls were hyper eosinophilic and homogenous consistent with fibrinoid necrosis. The lumen of affected vessels remained patent however without evidence for thrombosis (Figure 6E). In addition, no heat sink effect was evident adjacent to vessels with complete necrosis adjacent and often surrounding patent vasculature.

Nerves within the neurovascular bundles appeared to be intact and unaffected (figure 6E). Even ganglion cells showed no evidence of cells death.

The regional lymph nodes were enlarged in the drainage area. There was mild cortical reactivity and expansion of medullary sinuses consistent with a drainage reaction. Medullary sinuses are expanded by red blood cells, eosinophils, neutrophils, and macrophages. Para-cortical regions are expanded by increased lymphocytes. Occasional lymphoid follicles have reactive germinal centers.

At 2 weeks after the procedure the hemorrhagic changes had mostly resolved within the ablated tissue. The volume of tissue had already been markedly reduced compared to the untreated tissue. The contracted region of the previous lesion consisted primarily of collagenous tissue consistent with early scar formation (Figure 6B). Once again, the urethral wall adjacent to the lesion showed no evidence of necrosis and the urethral mucosa was intact. The nerves and vessels within the NVB on the side of the lesion were intact and patent. All layers of the rectum adjacent to the lesion appeared to be viable with no evidence for fistula formation.

The results of this study point to some of the advantages of NTIRE. First, the procedure obviously can produce prostate tissue ablation. The ability of NTIRE to ablate cells without destroying the extracellular matrix has major advantages in the case of the urethra, rectum and blood vessels. The sparing of the nerve may be related to the insulating nature of the myelin layer surrounding some nerves. Obviously, if this is the mechanism through which the nerves are spared any mechanical damage done to this layer or if pulses that break the insulating properties of the layer are delivered through a capacitance effect, the nerve cell may not be spared as evident from the early studies of [17].

NTIRE of the Heart and the Cardiovascular System

The ability of NTIRE to ablate cells without affecting the extracellular matrix may find important applications in ablation of cells for the cardiovascular system. One study in this area was performed by Dr. Liron Miller in the laboratory of Professor Jonathan Leor at the Sheba Hospital in Israel and was not reported in a reviewed publication.

Male Sprague-Dawley rats (150-200g) were obtained from (Harlan Lab. Jerusalem Israel) through the Office of Laboratory Animal Care at the Sheba Hospital, Israel. They received humane care from a properly trained professional in compliance with both the *Principals of Laboratory Animal Care* and the *Guide for the Care and Use of Laboratory Animals*, prepared and formulated by the Institute of Laboratory Animal Resources and published by the NIH. Four animals were treated. Each procedure started with anesthetization of the animal via intraperitoneal injection of 40 mg/kg ketamine and 10 mg/kg xylazine. Intubation was performed and the rats were ventilated with room air using a rodent ventilator. The chest was shaved under sterile conditions and surgically opened by left thoracotomy through the fourth intercostals space to expose the beating heart. Two electrodes were inserted into the heart at a depth of 4 mm. The 25 gage parallel electrodes were at a distance of 5 mm. The electrical fields were calculated as

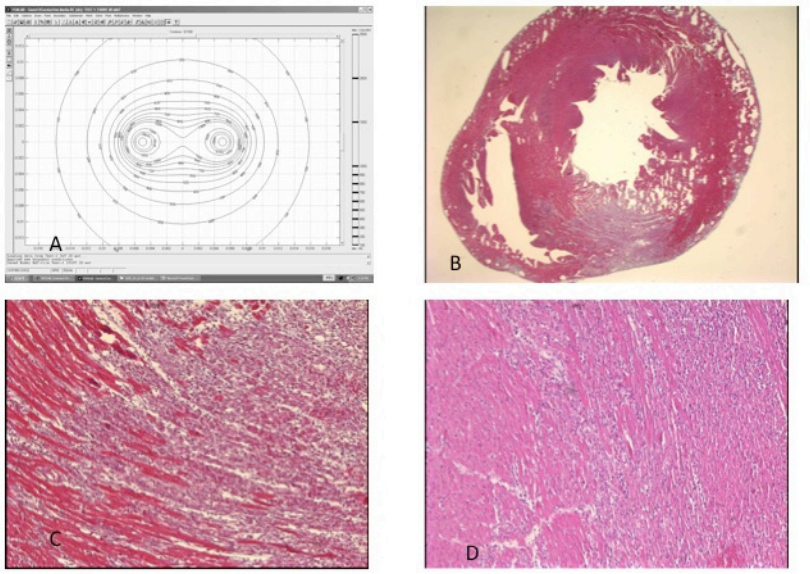

Fig. 7. 7A) Electrical fields that develop in the heart with two electrodes of gage 25, separated by 5 mm and a pulse of 750 V for 400 ms. The pulses were applied in the direction of the muscle fiber. 7B) Typical macroscopic cross sections through the heart in a plane parallel to that of electrode needles. He&E staining shows the necrotic region with a lighter color. 7C,7D Microscopic images of treated tissue in the heart. Figure 7c shows the margins of the treated areas. The muscle fibers that are alive ar shown as dark (red). The treated area has lost after 48 hours any living muscle fiber. It is evident from both that the entire treated area has been ablated and that the margins are very sharp, several cells thick.

shown in Fig. 7A and determined to produce non-thermal IRE. Two 400 microsecond pulses of 750 V, separated by 80 milliseconds were applied to the heart. The needles were placed perpendicular to the direction of the muscle fibers. The incision was sutured close and the animals recovered from anesthesia and were returned to their cages. The animals were maintained under observation for two days (48 hours) and than euthanized with an overdose of ketamine and xylazine. The hearts were removed, sectioned in the treated are and analyzed after embedding in paraffin and with imunohistochemical staining. Hematoxylin-eosin staining was performed on cross-sections through the center of the treated region to elucidate the morphology.

All the animals survived the procedure. The results are illustrated by Figs7 B,7C,7D. In Fig 7B, the cross section is through the heart in a plane parallel to the direction of the needles. The hematoxylin and eosin staining shows areas of heart tissue that are lighter. These areas correspond to the plane in which the needles were placed. Microscopic analysis, Figs 7C,7D shows that the lighter areas correspond to ablated tissue. Histological analysis revealed acute damage to the tissue in treated regions. Figure 7C shows the margins of the treated areas. The muscle

fibers that are alive are shown as dark (red). The treated area has lost after 48 hours any living muscle fiber. It is evident from both Figures 7C, 7D that the entire treated area has been ablated and that the margins are very sharp, several cells thick. The fact that the animals survived the procedure and where alive 48 hours later while in the treated area the cells became completely ablated is indicative of the unique attributes of NTIRE, which retains even crucial structures such as the extracellular structure of the heart while ablating cells.

Another important application of NTIRE in the heart is for tissue ablation in treatment of arrhythmias. A study on this application was reported in [17]. Five pigs underwent beating heart surgical epicardial ablations of their right and/or left atrial appendages, utilizing a sequence of 8, 16, or 32 direct current pulses of 1500 to 2000 V, 100 μs each, at a frequency of 5 per second, applied between two 4-cm long parallel electrodes (Figure 8A) with an IRE pulse generator. In 3 of the pigs, 2 ablations were performed on the left atrial appendage, 1 cm apart from each other, for a total of 10 atrial ablations. Temperature was measured at the left and right atrial appendages tips before, during, and after the pulse sequence applications with an EasyWay 15 Thermometer Datalogger (Extech Instruments, Waltham, MA, USA) and a type-K thermocouple. In 2 pigs, an electrical isolation study was performed following IRE ablation by pacing the tips of the left and right atrial appendages distal to the ablation lesions, at a stimulus strength of 20 mA, and capturing the heart response. All ablation pulse sequences were completed within 1 to 4 seconds, depending on the number of pulses within each sequence, and caused no permanent arrhythmia or any untoward rhythm disturbance apart from rapid atrial pacing during the pulse sequence application (Figure 8B). Local heat measurements at the left and right atrial appendages tips showed no temperature changes during the pulse sequence applications in any of the pigs. In the 2 pigs in which electrical isolation study was performed, complete electrical isolation was confirmed by pacing the tips of the left and right atrial appendages, distal to the ablation lesions, at a stimulus strength of 20 mA, and failure of the heart to capture. The sternotomy incision was then closed, and the pigs were extubated and followed for 24 hours, at which point they were euthanized. Animal hearts were excised 24 hours after surgery and stained with Masson trichrome staining to elucidate the myocardial damage. Degrees of myocardial damage (nuclear staining, homogeneity of myocytes striation), hemorrhage, or amount of inflammatory cells were studied. Complete myocardial necrosis was characterized by rounded, homogenous myocytes with loss of nuclear staining. Histological evaluation of lesion transmurality was based on maximum depth of myocardial necrosis. Complete transmural lesion was defined as myocardial necrosis throughout the atrial wall. On gross inspection of all 10 atrial lesions 24 hours after ablation, a clear demarcation line between ablated and normal tissue was observed, with no tissue disruption or charring (Figure 8C, 8D). Masson trichrome staining results of all 10 atrial ablations showed continuous transmural destruction of the atrial tissue—from epicard to endocard—at the site of the electrode application (Figure 8D). The 10 atrial lesions had a mean depth of 0.9 cm (range, 0.4-1.4 cm), mean width of 0.66 cm (range, 0.5-1.0 cm), and measured 3 to 3.5 cm in length. Higher

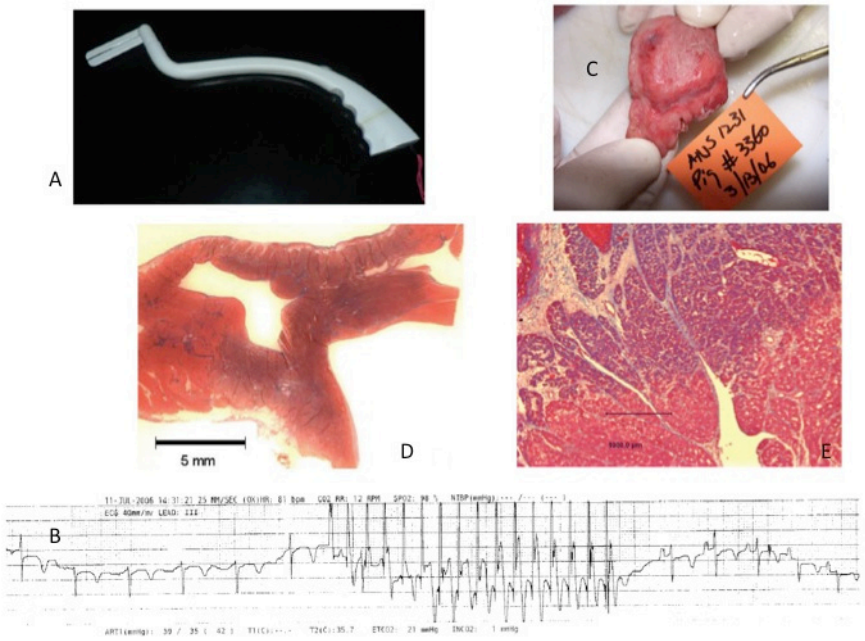

Fig. 8. 8A) A specially designed hand-held clamp containing 2 parallel electrodes embedded in its end jaws, which can be rotated at their handle articulation up to 270° to allow shaping of the device as the surgical situation requires and provide a clear visual field of the ablation site. 8B) Electrocardiographic tracing showing rapid atrial pacing during a 16-pulse irreversible electroporation ablation sequence, with a frequency of 5 pulses per second, and immediate resumption of sinus rhythm following ablation. 8C) Gross specimen of the left atrial appendage spread open, showing 2 clear linear ablation lesions on both sides of the appendage. 8D). Stereomicroscopy pictures of Masson trichrome stainings (original magnification ×2). Left atrial appendage lesion showing trans-mural lesion (in purple) from epicard to endocard. 8E) Higher magnifications of the ablated areas showing a sharp demarcation line between the injured necrotic myocardial tissue and the surrounding normal myocardium.

magnifications of the ablated areas have repeatedly demonstrated a sharp demarcation line between the injured necrotic myocardial tissue and the surrounding normal myocardium (Figure 8E). The study was the first to demonstrate the ability of IRE to serve as a surgical modality to create epicardial atrial ablation. Each of the 3- to 3.5-cm long transmural ablation lines were created in 1 to 4 seconds and caused no peripheral thermal damage. These features demonstrate the potential superiority of the IRE nonthermal modality over the currently used hyperthermic or hypothermic energy sources for future clinical application in the surgical treatment of atrial fibrillation.

An important aspect of NTIRE is that while ablating cells it keeps the extracellular matrix intact. In the case of blood vessels it means that the extracellular matrix remain mechanically intact with an intact molecular structure and mechanical

properties. This has suggested to us that NTIRE is an ideal modality for treating blood vessels for various applications, such as restenosis. A few studies on NTIRE for blood vessels were reported in [19], [20], [21]. A more comprehensive summary of the research can be found in the PhD thesis of Elad Maor [22]. All the animal studies were done performing first a mathematical treatment protocol to verify that the procedure is indeed non-thermal. The rat studies were performed as described in [19], [20], [21]. Animals were anaesthetized with an intramuscular injection of Ketamin and Xylazine (90mg/Kg and 10 mg/Kg, respectively). The left common carotid artery of each animal was exposed and a custom made electrode clamp with two parallel disk electrodes (diameter = 5 mm) was applied on the left common carotid artery (Figs 9a, 9b). A variety of studies on NTIRE are described in [19], [20], [21], [22]. One typical study evaluated the effectiveness of various NTIRE protocols. In that study, eight IRE protocols with different ways of delivering sequences of 100 μs in length were compared: 1-4) 10 pulses at a frequency of 10 Hz with electric fields of 3500, 1750, 875 and 437.5 V/cm and 5-8) 45 and 90 pulses at a frequency of 1 Hz with electric fields of 1750 and 875 V/cm. All groups had their left common carotid artery treated with NTIRE and their right common carotid artery used as a control. NTIRE was performed by applying short electric pulses between the electrodes with a high voltage pulse generator intended for electroporation procedures (ECM 830, Harvard Apparatus, Holliston, MA). The procedure was repeated in three successive locations along the common carotid artery, thus treating approximately 1.5 cm of the left common carotid artery. At the end of the procedure the skin incision was suture closed and animals were kept alive for various periods of time. For histological examination, animals were euthanized with an overdose of Phenobarbital followed by bilateral chest dissection. Gross inspection of carotid arteries was used to identify arterial wall integrity or intraluminal massive thrombus formation. The arterial tree was perfused with 10% buffered formalin, and the left and right carotid arteries were harvested near the bifurcation of the internal and external carotid arteries. The treated area was cut to two or three consecutive slices. One section from each slice was used for histological analysis. Each slice was fixed with 10% buffered formalin, embedded in paraffin, and sectioned with a microtome (5-μm-thick). Sections were stained with hematoxylin and eosin. Each section was photographed at ×200 magnification, and the following parameters were quantitatively evaluated: number of (vascular smooth muscle cells) VSMC nuclei in each of the three layers of the Tunica Media, total area of the Tunica Media, and the average thickness of the Tunica Media based on 5 different measurements in each section. Most efficient protocols were 10 pulses of 3500 V/cm at a frequency of 10 Hz and 90 pulses of 1750 V/cm at a frequency of 1 Hz, with ablation efficiency of 89±16 % and 94±9 % respectively. Extra-cellular structures were not damaged and the endothelial layer recovered completely. Typical histological results at one week after the application of successful NTIRE protocols that are shown in Fig 9d. In comparison Fig 9c shows a normal artery. The main aspect is that the VSCM cell were completely ablated and after one week, while there were no VCM cells, the endothelial cells started to regrow, in a normal fashion. This indicates the value of NTIRE and of the non-thermal aspect of the procedure. The extracellular matrix is retained and it

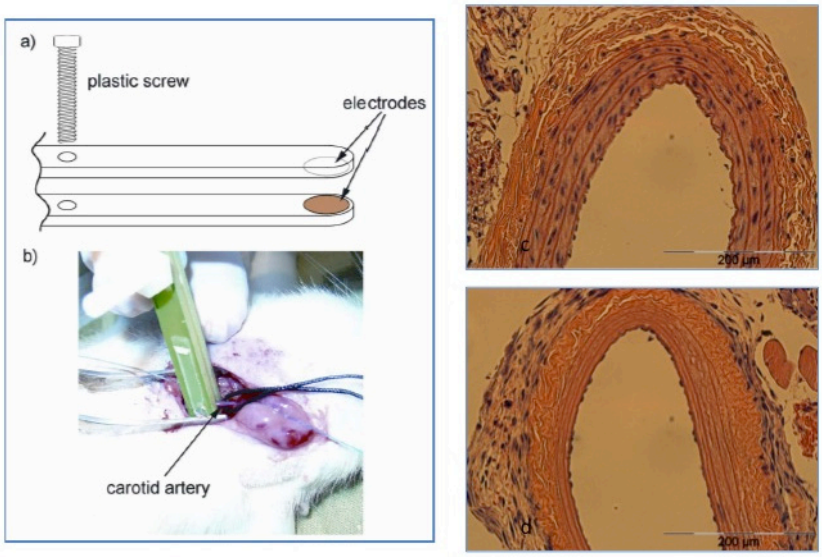

Fig. 9. 9a) a schematic of the electrodes for extra vascular treatment of the blood vessel. 9b) a typical procedure in which the blood vessels was clamped between the electrodes. 9c) a cross section through a control artery, 9d) a cross section of a treated artery a week after the treatment. Note the repopulation of the endothelial layer compared with the complete absence of the vascular smooth muscle cells. This is possible because of a unique aspect of NTIRE which ablates cells while retaining the extracellular matrix intact.

Successful NITRE ablation of VSMC induced a reduction in media thickness: 25±17% reduction in Group 1 (45±10 vs. 59±8 µm) and 27±7% reduction in Group 4 (37±4 vs. 51±6 µm) .No Change in media thickness was induced in the two non-successful NTIRE groups (61±9 vs. 58±7 µm in Group 5, 61±9 vs. 60±6 µm in Group 8). Endothelial cells of treated arteries were similar in number and morphology to those of non treated control arteries. Elastic fibers and wall integrity were preserved and similar to control arteries. There were no signs of local inflammation in treated arteries. There were no cases of bleeding, thrombosis and animal mortality.

In addition to the experiments described earlier we have performed a similar set of experiments with intravascular NTIRE electrodes in the rabbit (Figs 10). We tested several types of electrodes such as those shown in Figs 10 A and 10 B. Figure 10 C shows an angiograme of the left and right carotide artery four weeks after an angiography. The left was not treated with NTIRE after angiography while the right was. It is evident that the left artery has become completely occluded by the wild growth of smooth muscle cells while the right one is intact. This shows that NTIRE not only prevents neointimal formation but also negative vascular remodeling, without the need for a stent!

The evidence that NTIRE can ablate tissue around blood vessels suggests a wide range of applications related to the ablation of tissue around blood vessels

without affecting the extracellular matrix. For instance, tumors around blood vessels in the kidney, brain or pancreas could be treated in the same way, as well as direct treatment of soft plaque.

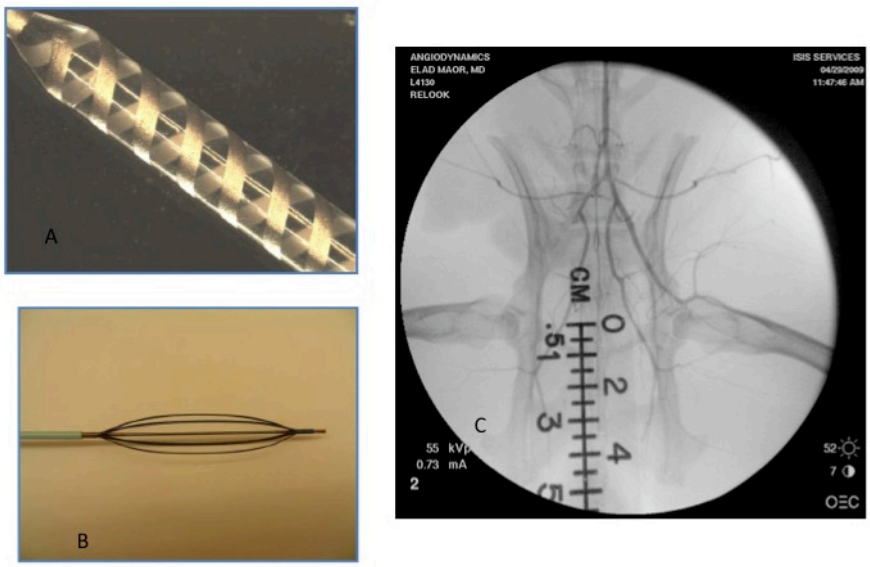

Fig. 10. 10A), 10B), typical intravascular NTIRE electroporation electrodes, 10 C) and angiogram of the rat carotid arteries one month after they were damaged by angiography. The right was treated with NTIRE and the left not. Note that the left has become closed and the right is intact.

NTIRE in the Treatment of Tumors

The first successful use of NTIRE irreversible electroporation for the minimally invasive treatment of aggressive cutaneous tumors implanted in mice was performed in the laboratory and under the direction of Lluis Mir and reported in [23]. Mathematical models of the electrical and thermal fields that develop during the application of the pulses were used to design an efficient treatment protocol with minimal heating of the tissue. Tumor regression was confirmed by histological studies, which also revealed that it occurred as a direct result of irreversible cell membrane permeabilization. Parametric studies show that the successful outcome of the procedure is related to the applied electric field strength, the total pulse duration as well as the temporal mode of delivery of the pulses. The best results were obtained using plate electrodes to deliver across the tumor 80 pulses of 100 μs at 0.3 Hz with an electrical field magnitude of 2500 V/cm. These conditions induced complete regression in 12 out of 13 treated tumors, (92%), through irreversible electroporation and in the absence of tissue heating. The study was performed on C57Bl/6 female mice, 6–8 weeks old, inoculated subcutaneously in the left flank

with $1x10^6$ cells from a LPB cell line, a methylcholanthrene-induced C57Bl/6 mouse sarcoma cell line, producing in 9 days tumors of 4 to 5mm in diameter. For electroporation, the mice were anaesthetized using a mixture of xylazine 12.5 $mg.kg^{-1}$ (Bayer Pharma, Puteaux, France) and ketamine 125 $mg.kg^{-1}$ (Parke Davis, Courbevoie, France), an incision was performed on the skin near the tumor and the skin flap containing the tumor was lifted and stainless-steel plate electrodes were placed in direct contact with both sides of the cutaneous tumor, with the tumor sandwiched between the parallel plates. After delivery of the electroporation pulses, the skin incisions were closed with metallic clips, the mice were returned to their cages and the evolution of the treated tumors was followed with measurements of tumor size every second day. Alternatively, mice were kept for different periods of time (between 1 and 72h) and then humanely sacrificed by CO_2 inhalation before the tumors were removed and processed for histological or immunohistochemical analysis.

The analysis involved haematoxylin–eosin-saffron (HES) staining in which tumors were fixed in Finefix (Milestone, Italy) and embedded in paraffin. Sections of 4µm were prepared for routine HES staining.

For immunohistochemistry of microvessels CD31 paraffin sections (4µm-thick) were dewaxed and rehydrated. Endogenous peroxidase activity was quenched by 3% H_2O_2 for 10min. Sections were placed in cover-plates (Shandon, Life Sciences Technology, Cergy-Pontoise, France) and incubated with blocking serum Power Block 1:10 (BioGenex, San Ramon, CA, USA) for 10min. The slides were then incubated for 1h with purified rat-anti-mouse monoclonal anti-platelet endothelial cell adhesion molecule (PECAM-1 also called CD31), dilution 1:300, (PharMingen, Heidelberg, Germany) followed by rabbit anti-rat immunoglobulins (Dako Denmark) dilution 1:200, for 30min, followed by PowerVision poly-HRP anti-Rabbit IgG (Immuno Vision Technologies, Brisbane, CA) for 20min. Finally, slides were exposed to diaminobenzidine chromogenic substrate (DAB PowerVision Histostaining Kit; ImmunoVision Technologies) for 10min, washed with distilled water, counterstained with Mayer's hematoxylin, and mounted in permanent medium (Pertex). All slides were immunolabelled the same day to ensure standardized intensities of immunochemical signals and counterstaining.

Double Strand DNA breaks, which are often associated with cell apoptosis, were detected using the "In Situ Cell Death" Detection kit (Roche; Mannheim, Germany) (TUNEL*(Terminal deoxynucleotidyl transferase (TdT)-mediated dUTP Nick End-Labeling)* method) performed according to the manufacturer's instructions. De-paraffinized sections were incubated with Citrate buffer, pH 6 and placed in a water-bath, 98°C for 40min and all sections were treated with TUNEL reagents (TUNEL mixture: 1 hour at 37°C under a coverslip) except for one where the enzyme was omitted (negative control). After washings with Rince Buffer Biogenex, slides were incubated with the secondary anti-fluorescein-AP conjugate, and the signal was revealed with Fast Red substrate solution for 20min. Slides were lightly counterstained with hematoxylin prior to aqueous mounting by Aqua-Perm (Shandon Aqua-Perm™ Thermo Electron IVDD Compliant, Waltham, MA).

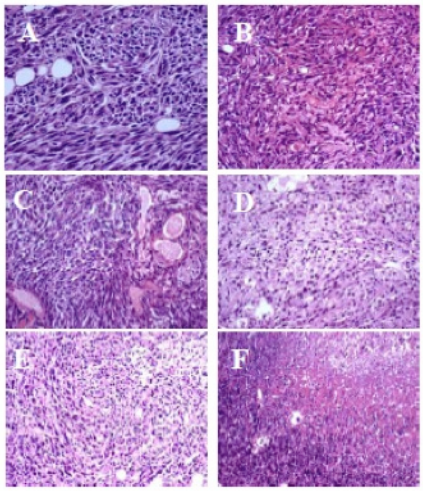

Fig. 11. Analysis of tumor evolution by HES histological staining after IRE. A: control; B, C, D, E and F: respectively 1, 2, 6, 24 and 48h after irreversible electroporation.

Figures 11 shows typical results from HES staining experiments. In the untreated control tumors, cells display a large nucleus surrounded by a well marked cytoplasm and a well defined cell membrane (Fig 11A). The slides stained with the classical HES staining revealed that 5 min after the EP, no change in tumour cell morphology was detectable. However, the congestion of blood in the tumour vessels was evident. This effect is similar to the irreversible electroporation consequences in the liver described in [3]. Few changes in tissue architecture and cell morphology were detected 1h and 2h later (Fig 11B and 11C). However, 6h after the EP, dramatic changes were observed (Fig 11D). Cytoplasmic limits between the cells were barely distinguishable in several parts of the tumour. The nuclei were still visible, but in a sort of syncitium in these parts of the tumour. At 24h, almost the entire tumor presented this image (Fig 11E). The nuclei, extremely pycnotic, appeared to be all in the same "cytoplasm" as no limit was detectable between the original cells. At 48h (Fig 11F) and 72h, the nuclei were even smaller and tissue necrosis still more evident.

Figures 12 show the results from both, Tunel staining, left panel and CD31 staining right pannel. TUNEL staining revealed that in the control slides, very few cells were stained positive. The staining was strictly localized at the level of the cell nucleus (Fig 12A). Background was very clear (Fig 4A). However, as early as 5min after the treatment, changes began, albeit slightly noticeable: a larger number of nuclei were positive, and in many of these nuclei, staining was not contained inside the nucleus, but was clearly spreading in the cytoplasm (Fig 12B). Background was still very clear (Fig 12B). The overall staining of the slices increased 1h after EP delivery. There was a clear increase in the number of red-dye leaking cells and there was

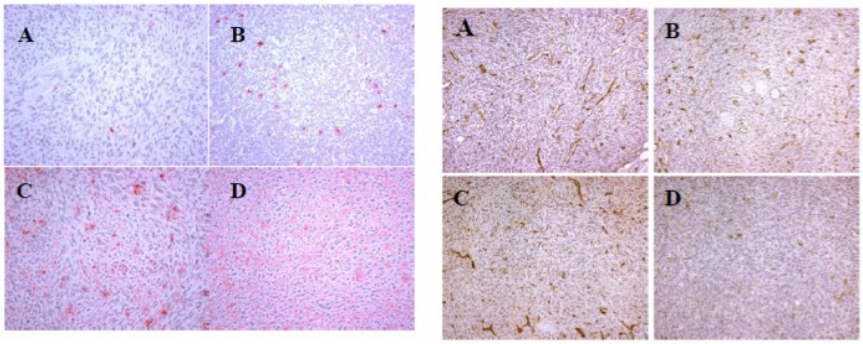

Fig. 12. Left hand side panel. TUNEL analysis at different times after the pulses delivery. A: control; B, C and D: respectively 5 min and 1 and 24h after IRE. Right hand side pannel: Immunohistochemical analysis of the tumour vasculature evolution by means of CD 31 staining in LPB tumors after treatment. A: control; B, C and D: respectively 2, 6 and 24h after IRE.

also the presence of a red background (Fig 12C). Thus, two types of staining can be clearly identified in these slices and at later times. At 6h, a large number of cells still display the diffuse staining (not shown). However, at longer times (24h, Fig 12D), there was only a heavily red-stained background, which completely diffused and continued to spread throughout the entire tumor section. At 24h, no more red-dye leaking cells were found, in agreement with the HES images that showed the complete disintegration of the cells.

Evolution of the tumor vasculature was also analyzed using antibodies against the CD31 endothelial cells specific marker, right panel. The changes in vasculature, which were observed 5 min after EP delivery were slight with respect to the controls (Fig. 12A), displayed highly branched and tortuous vasculature typical to this well vascularized fibrosarcoma tumor. However, 2h later, well established vascular congestion with dilated vessels was detectable, long vessels were not visible and a slight diffuse staining began to spread in some parts of the slices. At 6h, blood vessel walls, when still present, were either hyper- or hypo-pigmented. The diffusion of the CD31 marker in the extra-cellular interstitial spaces was much more intense and micro-vascular occlusions were also detectable. These signs indicate advanced tumour vasculature lesions. At 24h, very advanced vascular lesions were seen, with faint CD31 marker staining of the endothelial cells indicating damaged blood vessel walls, and intense diffusion of the staining in the whole tissue. What remained were blood vessel skeletons over a necrotic background.

The results achieved with the different sets of electrical parameters indicate that the main parameter affecting the results is the electric field strength. Trains of a large number of short pulses resulted in the best antitumor effects (up to 92% of tumor ablation).

This study has produced several observations concerning the mechanisms of cell ablation in the IRE method as well as evidence of the efficacy of IRE to completely destroy aggressive tumors. HES staining revealed that the IRE pulses induce vascular congestion, which should also cause tissue hypoxia and may further contribute to tumor cell death. Twenty-four hours after the application of the pulses, all treated tissue was necrotic. Interestingly, the treatment does not produce massive apoptosis. The number of nuclei stained by the TUNEL reaction slightly increases 1h after the treatment. The detection of diffused TUNEL staining first in the cytoplasm around the cell nucleus, and later around the cells, is consistent with the expected effects of IRE pulses. The observation of a diffused TUNEL staining of DNA corroborates that cells are no longer limited by their natural membrane barrier and the DNA diffuses outside the cell, which is indeed the hallmark of irreversible electroporation.

The analyses of the CD31 staining show rapid and severe lesions of the vasculature. At this stage it should be emphasized that the vasculature of these tumors is substantially different from the vasculature of normal major blood vessels. The blood vessels here have no inherent mechanical integrity and extracellular scaffolding. The results in [22] reveal that the disaggregation of the membranes starts a couple of hours after the pulse delivery and becomes very intense 6 h later, and is complete at 24 h. The localization of the membrane antigen CD 31 at the cell membrane is progressive and becomes complete. The antigen diffuses throughout the treated tumor volume, indicating the complete disruption of the membranes as well as cell necrosis. It is worthy to note that TUNEL analysis of the cell death and CD31 analysis of the tumor vasculature evolution revealed not only the necrotic pathway of the IRE-caused cell death, but also confirms the mechanisms of the method, that is the actual irreversible electroporation of the cell membrane and its consecutive disintegration.

Similar results to those discussed above were achieved with tumors transplanted in nude mice to assess whether the host immune system has a low or moderate participation in the antitumor effects observed. A supplementary study confirmed that the immune response is not instrumental for IRE ablation, which broadens the potential application space for IRE treatment to immunodepressed patients [24].

Summary of Experimental Studies

Several general conclusions emerge from the experimental studies performed so far. Non-thermal irreversible electroporation appears to be an effective tissue ablation modality. However, the procedure requires careful design of the many electroporation parameters that affect the outcome of the procedure. These involve a choice of number of pulses, pulse length, pulse amplitude and interval between pulses that will produce non-thermal irreversible electroporation. Since the number of parameters that are involved in the procedure is large, much research remains to be done to optimize the NTIRE protocol. A unique aspect of NTIRE is its

ability to ablate cells while the extracellular matrix remains intact. We anticipate that on the strength of this property NTIRE will find applications in areas in which no other minimally invasive surgical procedure was successful so far. Contractions during the electroporation pulses affect electroporation in general and irreversible electroporation in particular. This area needs to be further studied and at this stage considered whenever a clinical procedure is tested. The large animal experiments show evidence of a systemic immune response. It may be valuable to consider this response and ways to take advantage of it in treatment of cancer.

References

[1] Davalos, R., Mir, L., Rubinsky, B.: Tissue ablation with irreversible electroporation. Annals Biomed. Eng. 33(2), 223–231 (2005)
[2] Granot, Y., Rubinsky, B.: Mass transfer model for drug delivery in tissue cells with reversible electroporation. Int. J. of Heat and Mass Transfer 51, 5610–5616 (2008)
[3] Edd, J.F., Horowitz, L., Davalos, R.F., Mir, L.M., Rubinsky, B.: In-vivo results of a new focal tissue ablation technique: irreversible electroporation. IEEE Trans. on Biomedical Engineering 53(4), 1409–1415 (2006)
[4] Rubinsky, B., Onik, G., Mikus, P.: Irreversible Electroporation: A New Ablation Modality - Clinical Implications. Technology in Cancer Research and Treatment 6(1), 37–48 (2007)
[5] Gilbert, J.C., Onik, G.H., Haddick, W.K., Rubinsky, B.: The Use of Ultrasonic Imaging for Monitoring Cryosurgery. IEEE Trans. of Biomed. Eng. BME-31(8), 563 (1984)
[6] Gilbert, J.C., Onik, G.M., Haddick, W., Rubinsky, B.: Real Time Ultrasonic Monitoring of Hepatic Cryosurgery. Cryobiology 22, 319–330 (1985)
[7] Ivorra, A., Rubinsky, B.: In vivo electrical impedance measurements during and after electroporation of rat liver. Bioelectrochemistry 70(2), 287–295 (2006)
[8] Granot, Y., Ivorra, A., Maor, E., Rubinsky, B.: In vivo imaging of irreversible electroporation by means of electrical impedance tomography. Phys. Med. Biol. 21, 54(16), 4927–4943 (2009)
[9] Davalos, R., Rubinsky, B.: Temperature considerations during irreversible electroporation. Int. J. of Heat and Mass Transfer 51, 5617–5622 (2008)
[10] Daniels, C., Rubinsky, B.: Electrical Field and Temperature Model of Nonthermal Irreversible Electroporation in Heterogeneous Tissues. J. of Biomech. Eng. - Trans. of ASME 131(7), Article Number: 071006 (2009)
[11] Miklavcic, D., Semrov, D., Mekid, H., Mir, L.M.: A validated model of in vivo electric field distribution in tissues for electrochemotherapy and for DNA electrotransfer for gene therapy. Biochimica et Biophysica Acta 1523, 73–83 (2000)
[12] Martin, J.B., Young, J.L., Benoit, J.N., Dean, D.A.: Gene Transfer to Intact Mesenteric Arteries by Electroporation. Journal of Vascular Research 37, 372–380 (2000)
[13] Ivanusa, T., Beravs, K., Cemazar, M., Jevtic, V., Demsar, F., Sersa, G.: MRI macromolecular contrast agents as indicators of changed tumor blood flow. Radiol. Oncol. 35, 139–147 (2001)
[14] Sersa, G., Krzic, M., Sentjurc, M., Ivanusa, T., Beravs, K., Kotnik, V., Coer, A., Swartz, H.M., Cemazar, M.: Reduced blood flow and oxygenation in SA-I tumours after electrochemotherapy with cisplatin. British Journal of Cancer 87, 1047–1054 (2002)

[15] Sersa, G., Cemazar, M., Miklavcic, D.: Tumor blood flow modifying effects of electrochemotherapy: a potential vascular targeted mechanism. Radiol. Oncol. 37, 43–48 (2003)
[16] Onik, G., Mikus, P., Rubinsky, B.: Irreversible electroporation: Implications for prostate ablation. Technology in Cancer Research and Treatment 6(4), 295–300 (2007)
[17] Stämpfli, R., Willi, M.: Membrane potential of a ranvier node measured after electrical destruction of its membrane. Experimentia 13, 297–298 (1957)
[18] Lavee, J., Onik, G., Mikus, P., Rubinsky, B.: Novel Non-Thermal Energy Source for Surgical Epicardial Atrial Ablation: Irreversible Electroporation. The Heart Surgery Forum 10(2), E162–E167 (2007)
[19] Maor, E., Ivorra, A., Leor, J., Rubinsky, B.: The effect of irreversible electroporation on blood vessels. Technology in Cancer Research and Treatment 6(4), 307–312 (2007)
[20] Elad, M., Antoni, I., Leor, J., Boris, R.: Irreversible Electroporation Attenuates Neointimal Formation after Angioplasty. IEEE Trans. Biomed. Eng. 55(9), 2268–2274 (2008)
[21] Maor, E., Ivorra, A., Rubinsky, B.: Non Thermal Irreversible Electroporation: Novel Technology for Vascular Smooth Muscle Cells Ablation. PLoS ONE 4(3), e4757 (2009), doi:10.1371/journal.pone.0004757
[22] Maor, E.: Fundamental study on the effects of irreversible electroporation pulses on blood vessels with application to medical treatment. PhD Thesis, University of California at Berkeley (2009)
[23] Al-Sakere, B., André, F., Bernat, C., Connault, E., Opolon, P., Davalos, R., Rubinsky, B., Mir, L.: Tumor Ablation with Irreversible Electroporation. PLoS ONE 2(11), e1135 (2007)
[24] Al-Sakere, B., Bernat, C., André, F., Connault, E., Opolon, P., Davalos, R.V., Mir, L.M.: A study of the immunological response to tumor ablation with irreversible electroporation. Technology in Cancer Res. Treat. 6, 301–306 (2007)